Supplementary Information

$U_2N@I_h(7)$-C_{80}: Fullerene Cage Encapsulating An Unsymmetrical U(IV)=N=U(V) Cluster

Xiaomeng Li,[a†] Yannick Roselló,[b†] Yang-Rong Yao,[c†] Jiaxin Zhuang,[a] Xingxing Zhang,[a] Antonio Rodríguez-Fortea,[b] Coen de Graaf,[b,d] Luis Echegoyen,[c] Josep M. Poblet,[b] Ning Chen[a*]

[a.] College of Chemistry, Chemical Engineering and Materials Science, Soochow University, Suzhou, Jiangsu, 215123 (P. R. China)

[b.] Departament de Química Física i Inorgànica, Universitat Rovira i Virgili, 43007, Tarragona (Spain)

[c.] Department of Chemistry, University of Texas at El Paso, 500 West University Avenue, El Paso, Texas 79968,(United States)

[d.] ICREA, Passeig Lluís Companys 23, Barcelona (Spain)

Table of Contents

High-performance liquid chromatography (HPLC) separation process of $U_2N@I_h(7)$-C_{80}. The first stage was performed on a Buckyprep-M column (25 mm × 250 mm, Cosmosil Nacalai Tesque) with toluene as mobile phase. After that, as shown in Figure S1, fraction from 52 to 65 min (marked in blue) was re-injected into a Buckyprep-D column (10 mm × 250 mm, Cosmosil Nacalai Tesque) for the second stage separation

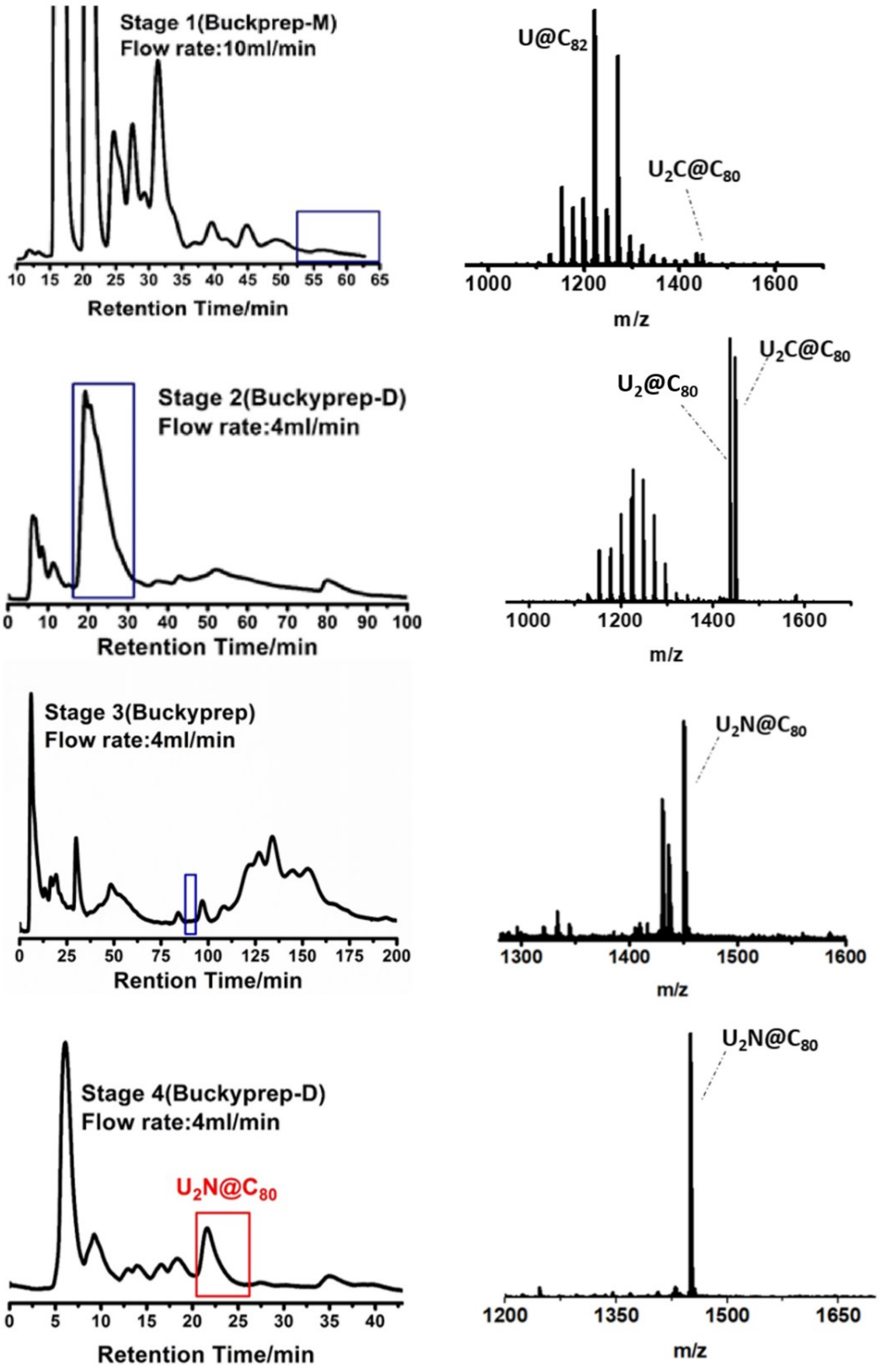

Figure S1. HPLC profiles showing the separation procedures of $U_2N@I_h(7)$-C_{80}(left) and the corresponding MALDI-TOF mass spectra (right).

using toluene as the eluent. The fraction marked in blue was collected (16-31min). The third stage of separation was conducted on a Buckyprep column (10 mm × 250 mm, Cosmosil Nacalai Tesque) using toluene as the eluent. As can be seen from the MALDI-TOF mass spectra, no signal of $U_2N@C_{80}$ was observed after these two stages, which is because the percentage of $U_2N@C_{80}$ was too low and the mass peak was covered by the isotopic distribution of $U_2C@C_{80}$. The third stage of separation was conducted on a Buckyprep column (10 mm × 250 mm, Cosmosil Nacalai Tesque) using toluene as the eluent and the fraction marked in blue was collected(82-92min). The final stage of separation was conducted on a Buckyprep-D column (10 mm × 250 mm, Cosmosil Nacalai Tesque) with toluene as the eluent and pure $U_2N@C_{80}$ was got.

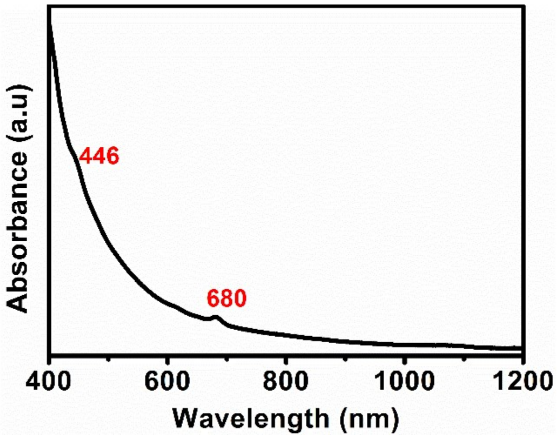

Figure S2. UV-Vis-NIR absorption spectrum of $U_2N@I_h(7)$-C_{80} in CS_2 solution

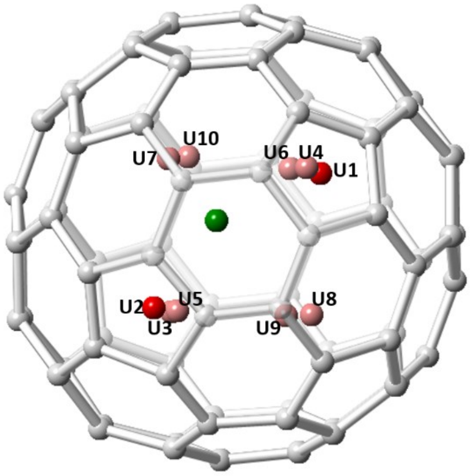

Figure S3. The perspective drawing showing the disorder of U in the $I_h(7)$-C_{80} cage.

Table S1. Occupancies of disordered uranium in $U_2N@I_h(7)$-C_{80}.

site	U1	U2	U3	U4	U5	U6	U7	U8	U9	U10
occupancy	0.86	0.86	0.05	0.05	0.03	0.03	0.05	0.05	0.01	0.01

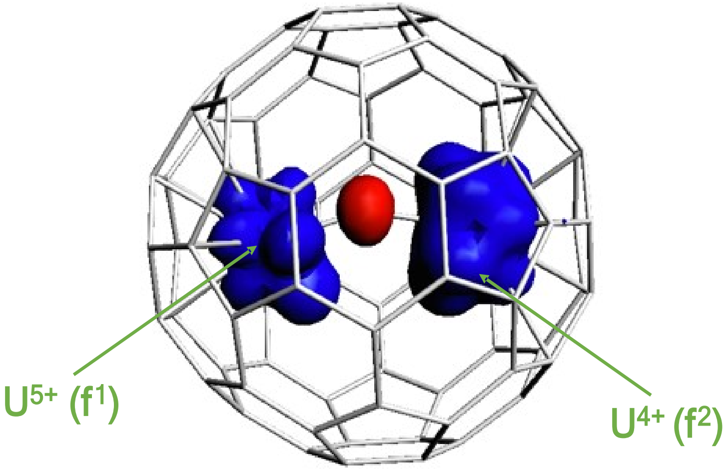

Figure S4. Spin density distribution computed at PBE0 for $U_2N@I_h(7)$-C_{80}.

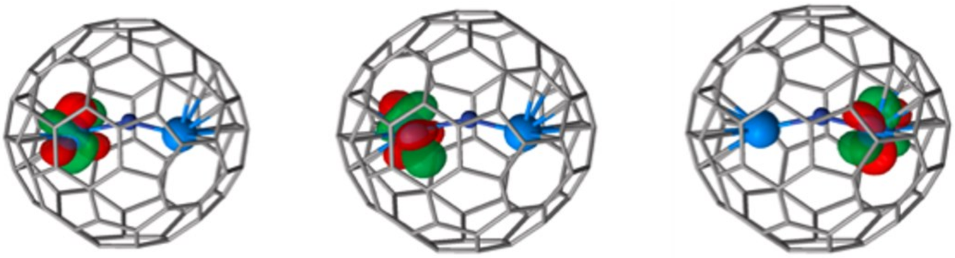

Figure S5. Single electron occupied CASSCF f orbitals computed for $U_2N@C_{80}$.

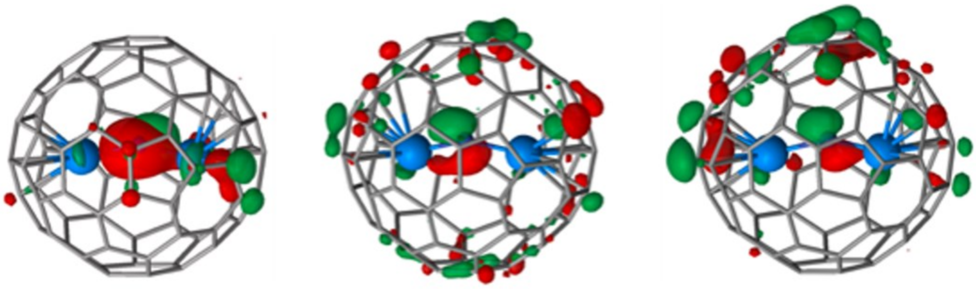

Figure S6. Selected CASSCF for $U_2N@C_{80}$ exhibiting some pi interaction between N(2p) and U(5f/6d) orbitals.

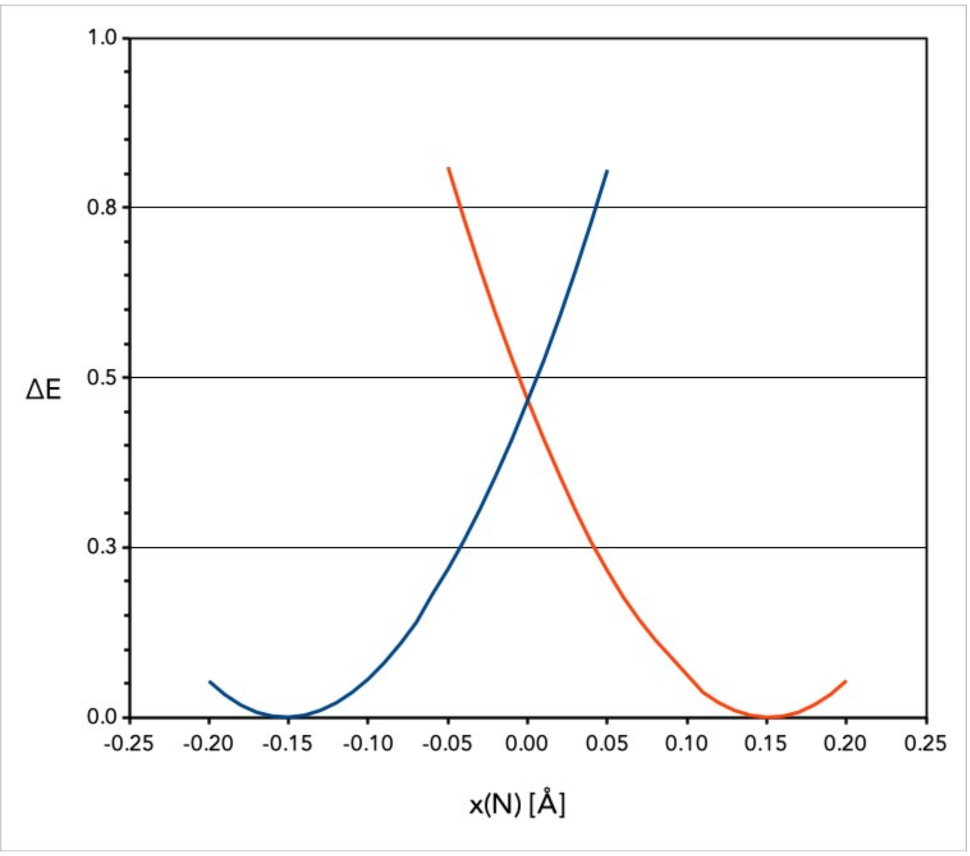

Figure S7. CASPT2 energy (in eV) of the ground state as function of the displacement of the central N-atom along the U—U axis for the $(NH_2)_3UNU(NH_2)_3$ model. The red curve represents the electronic state with a U^{4+}—N—$U^{5+,}$ the blue curve represents the opposite situation with a U^{5+}—N—U^{4+} distribution. The strong orbital relaxation around the differently charged uranium atoms makes the blue curve remain a 'deep' local minimum for positive x, falling onto the red curve requires a substantial amount of orbital reorganization. At x=0, there is in principle an interaction between the blue and red electronic states, <blue | H | red >, which would change the curve crossing into an avoided crossing. However, this interaction is so small that using the energies arising from the state interaction does not visibly change the graph.

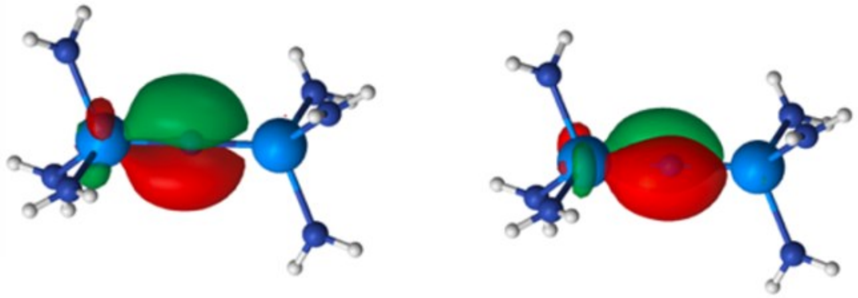

occ. nu. = 1.96

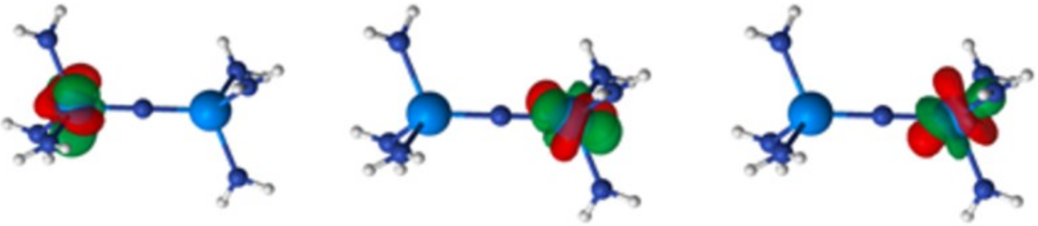

occ. nu. = 1.00

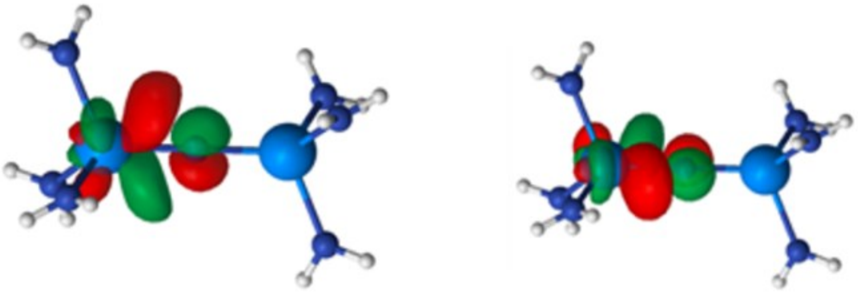

occ. nu. = 0.04

Figure S8. CASSCF active orbitals (7,7) for the $(NH_2)_3UNU(NH_2)_3$ model.

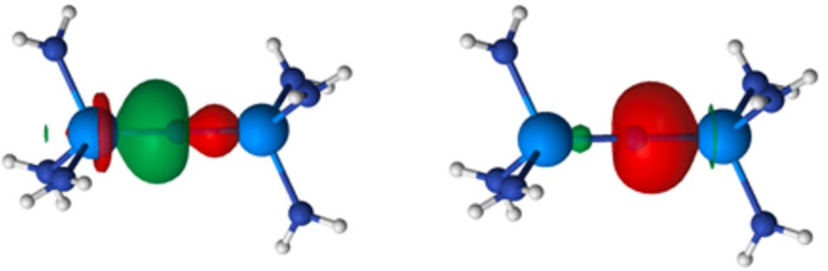

Figure S9. Localized CASSCF sigma orbitals for the $(\text{NH}_2)_3\text{UNU}(\text{NH}_2)_3$ model.

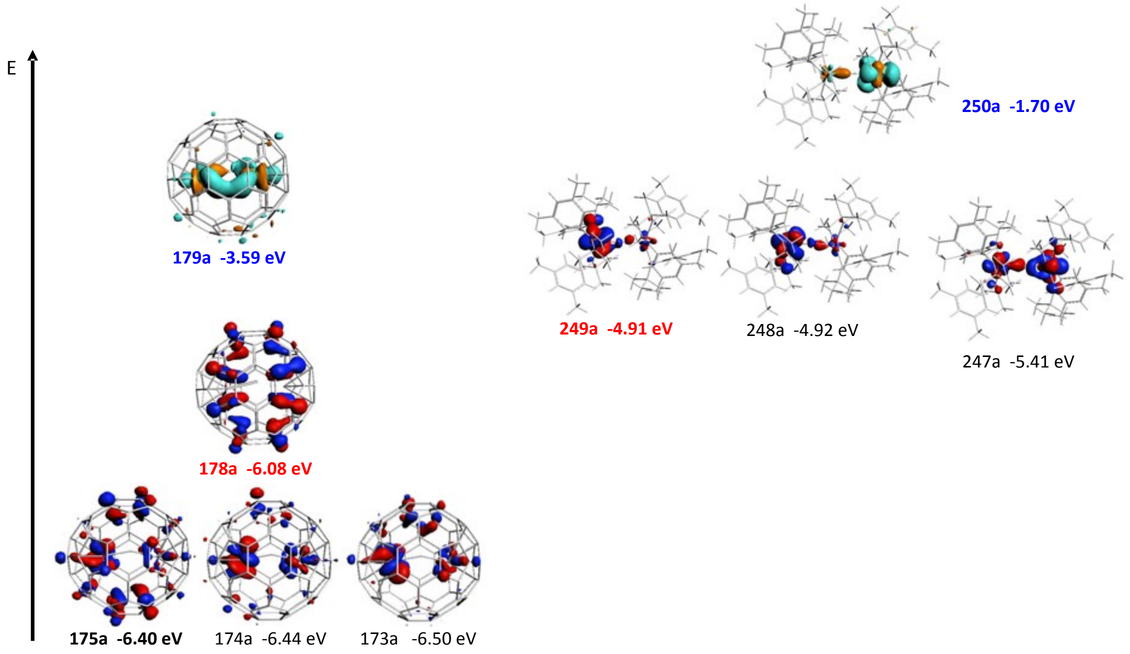

Figure S10. Comparison of PBE0/TZP canonical frontier orbitals for $\text{U}_2\text{N@C}_{80}$ (left) and $(\mu\text{-N})(\text{U}(\text{N}^t\text{BuAr})_3)_2$ (right). Although the HOMO in the endofullerene is delocalized over the cage the oxidation occurs in the U^{IV} ion.

Table S2. Energies and Composition (% on U1, X and U2) of the Localized MO for U_2X Inside $I_h(7)\text{-C}_{80}$ (X= C, N and O). [a)]

LMO	**X=C**				**X=N**				**X=O**			
	ε	**U1**	**X**	**U2**	**ε**	**U1**	**X**	**U2**	**ε**	**U1**	**X**	**U2**
π_1	-10.17	19.2	60.0	19.9	-12.54	16.4	73.1	8.1	-15.38	5.9	86.9	4.2
π_2	-10.46	20.0	60.0	20.0	-13.11	17.3	74.7	7.6	-15.92	6.2	86.2	4.5
σ_1	-13.09	3.7	66.4	26.7	-15.50	1.7	79.1	13.5	-18.06	0.3	88.9	4.2
σ_2	-13.14	26.8	66.2	3.0	-16.43	22.3	72.0	1.4	-18.21	5.4	88.5	0.9

a) Orbital energies in eV.

Table S3. Comparison of experimental bands in the IR and Raman spectra for $U_2N@I_h(7)-C_{80}$ and calculated vibrational frequencies for some of its normal modes of vibration.

□$_{\mathbf{exp}}$ (cm^{-1})	**□$_{\mathbf{calc}}$ (cm^{-1})**	**Description of the NMV**
-	31	Frustrated rotational mode of U_2N inside the cage
-	36	Frustrated rotational mode of U_2N inside the cage
-	53	Frustrated translational mode of U_2N inside the cage
-	56	Frustrated translational mode of U_2N inside the cage
126	116	U-N-U bending
	133	
-	156	Frustrated translational mode of U_2N inside the cage
-	210	Bending coupled to symmetric stretching and breathing mode of the cage
222	216	Breathing of the cage
	219	
238	237	Breathing of the cage
	239	
280	296	U-N-U symmetric stretching coupled to breathing of the cage
788	836	U-N-U asymmetric stretching

[a] The calculation was done using the PBE0 functional, SDD pseudopotential for U and 6-31G(g,p) basis set for N and C.

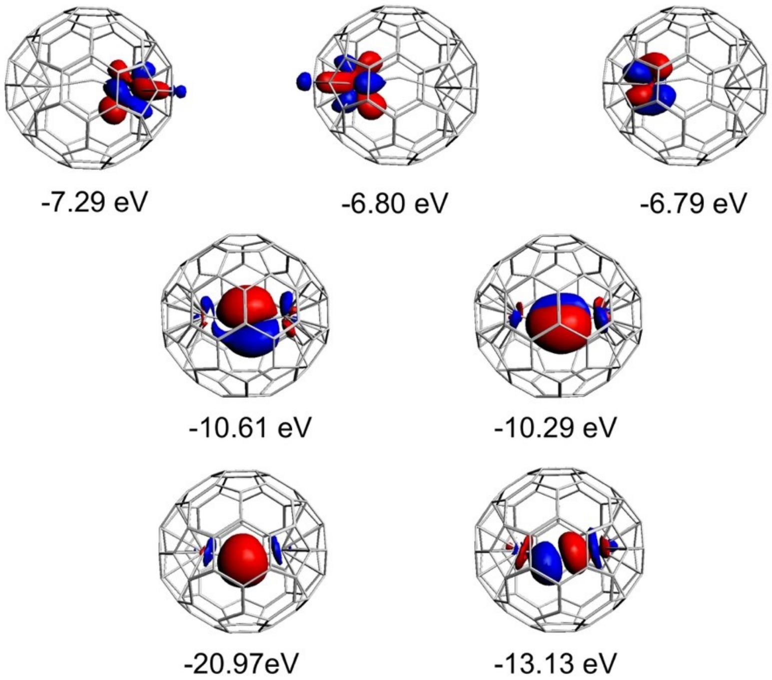

Figure S11. Localized (Pipek-Mezey) MOs for $U_2N@C_{80}$. LMOs relevant to bonding in U_2X moiety are represented. Orbital energies (in eV). In general, both Boys-Foster and Pipek-Mezey methods give very similar results for pi orbitals. With Pipek-Mezey, the sigma orbital is separated from the lone pair, while Boys-Foster gives two almost identical orbitals containing sigma and lone pair contributions. These apparently different pictures do not modify the general interpretation that can be obtained from the two localization algorithms.

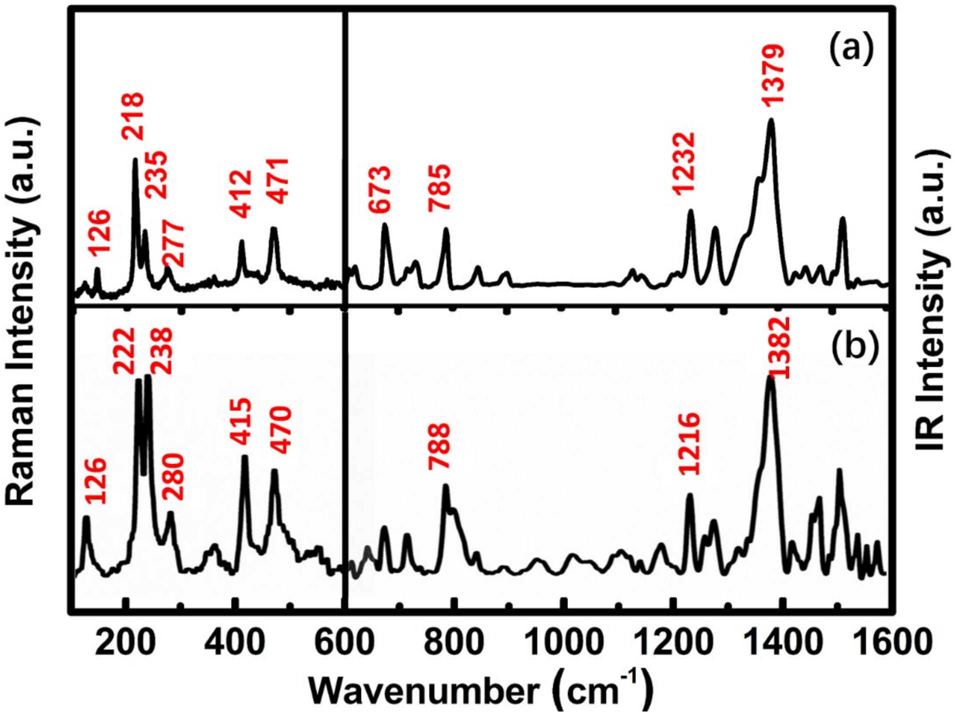

Figure S12. Comparison of IR and Raman spectra of (a) $U_2C@C_{80}$ and (b) $U_2N@C_{80}$.

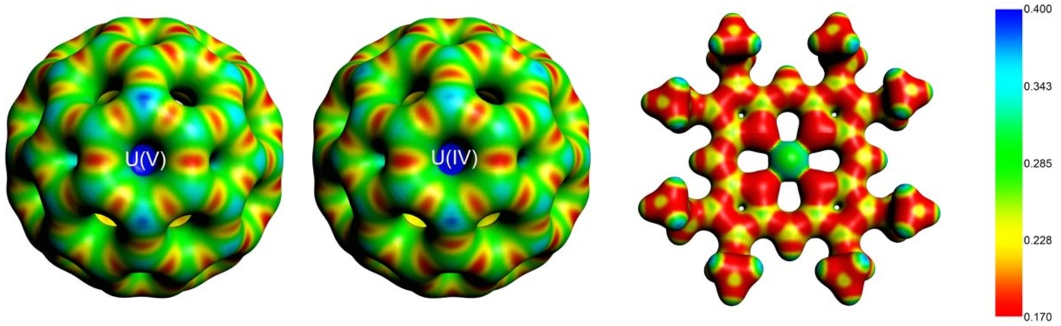

(a) (b) (c)

Figure S13. Two different views of the molecular electrostatic potential (MEP) of $U_2N@C_{80}$, (a) the hexagon nearest to U(V) is shown in front of the picture; (b) the hexagon nearest to U(IV) is shown in front of the picture; (c) MEP of the porphyrin (same scale as for the fullerene). No significant differences between the region of the fullerene nearby U(V) and that nearby U(IV) are found to explain that U(V) is placed much nearer to the NiOEP. In fact, we observe a kind of belt in the equatorial region far from the U atoms where the MEP is more negative, which in principle could have a more favorable electrostatic interaction with the Ni^{2+} of the porphyrin. By inspecting in detail the MEP in the region of the fullerene that is interacting with the porphyrin, we are not able to find a simple explanation for the interaction from a pure electrostatic point of view. We infer that the role of π-π interactions might be important here. A systematic study of the interaction between the fullerene and the NiOEP at different positions around the cage seems to be necessary to have more insights about this type of interaction.